Polyhedron 68 (2014) 191–198

Contents lists available at ScienceDirect

Polyhedron

journal homepage: www.elsevier.com/locate/poly

Water soluble diaza crown ether derivative: Synthesis and barium complexation studies

Leïla Boubekeur-Lecaque [a,*], Clément Souffrin [a], Geoffrey Gontard [b], Kamal Boubekeur [b], Christian Amatore [a]

[a] Department of Chemistry, UMR 8640 CNRS-ENS-UPMC, 24 rue Lhomond, 75005 Paris, France
[b] Institut Parisien de Chimie Moléculaire, UMR CNRS 7071, Université Pierre et Marie Curie, 4 Place Jussieu, 75005 Paris, France

ARTICLE INFO

Article history:
Received 10 September 2013
Accepted 22 October 2013
Available online 1 November 2013

Keywords:
Diaza-18-crown-6-ether
Barium
Affinity constant
Spectroscopy
Cation release

ABSTRACT

The combination of a mcrocyclic cavity with o-diaminobenzene derivative offers a new redox-active and water-soluble ligand for barium that incorporates 12 potential donors. The chelator was synthesized in four steps from diaza-18-crown-6-ether and fully characterized in solution by cyclic voltammetry, UV–Visible and NMR spectroscopies in the presence of barium. The corresponding complex exhibits a 1:1 stoichiometry in solution whereas it crystallizes as 3:2 (M:L) as evidenced by X-ray diffraction studies. The high affinity constant for barium estimated by NMR and electronic absorption techniques in aqueous medium, makes this ligand a promising candidate for redox-induced barium release.

1. Introduction

Calcium serves as a key signaling messenger in various biological processes such as intercellular communication [1,2]. The latter is made possible by the release of chemical messengers from an emitting cell to a target cell. For instance, the transmission in neurons is operated by neurotransmitters located in vesicles inside the emitting cell. The appropriate cell stimulation provoking a Ca^{2+} entry or increase, induces the docking of vesicles to the cell membrane followed by the fusion of the vesicle with the cell membrane and then the release and diffusion of the messenger in extracellular medium toward the neighboring cells [3]. This cascade of events known as vesicular exocytosis is biologically initiated by a significant increase in cytosolic Ca^{2+} concentration whose duration and concentration level are critical for the mechanism of vesicular fusion [4]. In vitro studies of exocytosis cascade require the stimulation of the emitting cells leading to an increase in intracellular free Ca^{2+} concentration. Among the various secretagogues *i.e.* stimulating agents that trigger exocytosis (Ca^{2+}/K^{+}, Ca^{2+}/nicotine, Ca^{2+}/digitonine, Ba^{2+}...), barium stimlation has retained our attention. Although not completely elucidated for all cells, it is firmly established that barium can efficiently substitute for Ca^{2+} and is able to induce secretion from a variety of cell types under Ca^{2+}-free conditions [5–7]. The protocol of stimulation with barium is very simple and consists in incubating the cell in a millimolar solution of Ba^{2+} in the absence of extracellular Ca^{2+}. However, Ba^{2+}-evoked release of neurotransmitters in such stimulation protocol is not spatially resolved as all regions of the cell are equally stimulated. Inspired by photo [8–10] and redox-induced [11,12] Ca^{2+} release strategies, we envisaged designing a selective redox-active barium chelator to deliver free barium as a secretagogue with high spatial and temporal resolution in extracellular medium. The oxidation or reduction of the redox reporter incorporated in the chelator provokes a charge and or/ a conformational modification that may affect sufficiently the binding ability of the ligand, thus favoring the release of a chelated ion.

The design of such selective chelator must fulfill strict requirements dictated primarily by biological constraints such as water solubility, physiological pH, and remarkable selectivity for barium over all other competing cations. Numerous exemples of selective barium ligands for sensing applications are reported in the litterature but most of them operate only in organic solvents [13,14]. The combination of macrocyclic cavities with redox-active units has been successfully exploited in organic solvents for sensing and redox-switchable applications. In particular, pioneering results with reducible subunits such as nitrobenzyl or quinone allowed the detailed description both theoretically and experimentally of the square-scheme mechansim that couples complexation and electron transfer reactions [14,15]. Oxidizable redox probes such as ferrocene, tetrathiafulvalene and phenylenediamine, were also combined to macrocycles for electrochemical cation sensing in organic solvents [16]. Few exemples of water-soluble chelating

* Corresponding author. Address: Laboratoire Interfaces, Traitements, Organisation et Dynamique des Systèmes (ITODYS), CNRS UMR 7086, Université Paris Diderot, 15 rue Jean-Antoine de Baïf, 75205 Paris Cedex 13, France. Tel.: +33 157278772; fax: +33 1 44323863.
E-mail address: leila.boubekeur@univ-paris-diderot.fr (L. Boubekeur-Lecaque).

0277-5387/$ - see front matter © 2013 Elsevier Ltd. All rights reserved.
http://dx.doi.org/10.1016/j.poly.2013.10.024

agents for Ba^{2+} based on crown ether motif and featuring phosphonate or carboxylate groups are known but they do not feature a redox probe [17,18]. Herein we describe the synthesis and characterization of a novel barium chelator combining diaza-18-crown-6 ether as the binding pocket, o-diaminobenzene as the redox probe and carboxylate side arms. Besides increasing the solubility in water, carboxylate groups, when ionized, provide strong electrostatic interaction with hard metals like alkali and alkaline earth cations. This new water soluble platform features 12 potential donors which corresponds to the higher coordination number encountered in barium coordination chemistry.

2. Material and methods

2.1. General considerations

All reactions were performed under argon if not stated otherwise and all chemicals were purchased from Sigma/Aldrich (France) or Alfa Aesar (France). Acetonitrile and DMF were distilled from CaH_2. ^1H and ^{13}C NMR spectra were recorded on Bruker AC-250 spectrometer in the solvents indicated at 298 K. Chemical shifts are reported using the deuterated (^{13}C NMR) or the residual monoprotonated (^1H NMR) solvent signals as reference. All coupling constants (*J* values) were measured in Hz. Elemental analysis were conducted at the Service de Microanalyses- ICSN (Gif sur Yvette, France). Thin layer chromatography (TLC) was performed on aluminium sheets precoated with 60 F_{254} silica gel. Preparative flash chromatography was performed on silica gel 60 (0.040–0.063 mm, Merck).

2.2. Electrochemistry

The electrochemical experiments were conducted in an air-tight three electrodes glass cell under argon atmosphere, controlled by a computer-controlled potentiostat (μ-Autolab, Eco-Chemie, the Netherlands). A large platinum wire and a saturated calomel electrode were used as a counter electrode and a reference electrode, respectively. A glassy carbon electrode with a disk radius of 0.5 mm, was used as working electrode and polished to a mirror finish before each experiment. Electrochemical studies in organic solvent were conducted in acetonitrile solutions of **3** (1 mM) containing either 0.1 M of $TBABF_4$ as a supporting electrolyte. The aqueous supporting electrolyte employed with the water soluble ligand **4** was prepared from ultra-pure water (<18 MΩ/cm) and contained 0.1 M $NaNO_3$, pH 7. Cyclic Voltammograms (CV) were recorded at room temperature (22 ± 2 °C) at a potential sweep rate of 0.1 V s^{-1}. Barium perchlorate was employed in organic electrolyte and barium chloride in aqueous electrolyte.

2.3. UV–Vis studies

All spectra were recorded on a computer-controlled Lambda 45-Perkin Elmer spectrophotometer. Spectroscopic measurements were performed in aqueous solutions at a constant ionic force set by 0.1 M $NaNO_3$, pH 7. UV–Vis studies for **4** (100 μM) were conducted by direct titration with sequential additions of a solution of $BaCl_2$ (or $CaCl_2$, $MgCl_2$, KCl) until full saturation is reached ([M]/[**4**] = 50 equivalents). After each concentration increment, the solution was stirred for 5 min to reach equilibrium before recording the UV–Vis spectrum. Data were analyzed at different wavelengths (263 and 239 nm) and the normalized absorbance $((A-A_0)/(A_0-A_{lim}))$ versus the ratio [M]/[**4**] plotted. Since the free cation concentration [M] could not be approximated by the total cation concentration c_M, the Benesi–Hildebrand model is not applicable. However, in the case of 1:1 complex stoichiometry, an explicit expression of the absorbance versus the total concentration c_M can be derived without approximation from the second order equation:

$$c_L.x^2 - (c_L + c_M + K_d).x + c_M = 0 \quad (1)$$

where: $x = \frac{A-A_0}{A_0-A_{lim}}$, A_0 (A_{lim}) is the absorbance at $c_M = 0$ (at full saturation respectively), A the absorbance at a given c_M, $c_M = [M]_{free} + [ML]$, $c_L = [L]_{free} + [ML]$ and K_d the dissociation constant. The explicit expression of the absorbance A versus c_M is a solution of the second order equation (Eq. 1). K_d can thus be obtained by a nonlinear least square minimization.

2.4. Determination of binding constant by ^1H NMR

For binding constant determination, ^1H NMR spectra were recorded in deuterated water at constant ionic force of 0.1 set by $NaNO_3$. Titration experiments were carried out by mixing the ligand solution in D_2O to a solution of barium chloride. Changes in the chemical shift of the methylenic protons adjacent to the carboxylate groups were exploited for the detrmination of binding constant. Data of $\Delta\delta$ (chemical shift variation) against $[Ba^{2+}]$ were fitted to a 1:1 binding model using origin 8.1 software (see Fig. S9 in the ESI).

$$\Delta\delta = \delta - \delta_0 = (\delta_{lim} - \delta_0).\frac{[ML]}{[L]_0}$$

Where $\Delta\delta$ is the measured change in chemical shift, δ_{lim} (and δ_0) is the chemical shift of the barium complex (and of the free ligand respectively). $[L]_0$ is the total concentration of ligand (free and complexed forms) and [ML] is the free barium concentration determined as a solution of the quadratic equation:

$$[ML]^2 + (-[L]_0 - [M]_0 - \frac{1}{K_a}) \cdot [ML] + [M]_0 \cdot [L]_0 = 0$$

Where $[M]_0$ is the pre-equilibrium barium concentration. Non linear curve-fitting of the experimental $\Delta\delta$ versus $[M]_0$ at a known $[L]_0$, yielded the parameters δ_{max}, K_a and [C].

2.5. Synthesis

2.5.1. Bis(2-nitrophenyl)-diazacrown ether **1**

(1,4,10,13)-Tetraoxa-7,16-diazacyclooctadecane (206 mg, 0.785 mmol), o-fluoronitrobenzene (175 μL, 1.65 mmol) and triethylamine (241 μL, 1.73 mmol) were dissolved in 2.5 mL of anhydrous DMF. The yellow solution was stirred for 6 h at 100 °C. The rsulting orange solution is concentrated under vacuum and diluted with dichloromethane and washed with aquous solution of $NaHCO_3$, water, then saturated solution of NaCl. The organic phase was dried on anhydrous Na_2SO_4, filtered then evaporated to dryness to give **1** yellow crystalline solid (696 mg, 90%).

^1H NMR (250 MHz, $CDCl_3$): δ 7.65 (dd, $^3J_{HH}$ = 8.1 Hz, $^4J_{HH}$ = 1.2 Hz, 2H), 7.31–7.51 (m, 4H), 6.93–7.04 (m, 2H), 3.61 (t, $^3J_{HH}$ = 5.3 Hz, 8H, $OCH_2\underline{CH_2}N$), 3.55 (s, 8H, OCH_2CH_2O), 3.47 (t, $^3J_{HH}$ = 5.3 Hz, 8H, $O\underline{CH_2}CH_2N$). ^{13}C NMR (62.5 MHz, $CDCl_3$): δ 145.1 (C^{Ar}–NO_2), 136.6 (C^{Ar}–$N_{ethercrown}$), 125.4, 123.4, 117.7 and 115.2 (C^{Ar}–H), 70.5, 54.7 and 69.0 (CH_2O and CH_2N). Elemental *Anal.* Calc. for $C_{24}H_{32}N_4O_8$: C, 57.13; H, 6.39; N, 11.10. Found: C, 56.77; H, 6.54; N, 11.48%.

2.5.2. Bis(2-aminophenyl)-diazacrown ether **2**

1 (400 mg, 0.793 mmol) and Pd/C (10%, 75 mg) were placed in a nitrogen flushed schlenk flask and suspended in 7 mL of ethanol. A slow flow of H_2 was bubbled in the reaction mixture until the solu-

tion turned colorless. After purging with argon, the suspension was fltered through Celite and the pad washed with dichloromethane. The filtrate was evaporated to dryness to give a colorless solid residue.

^{1}H NMR (250 MHz, $CDCl_3$): δ 7.05–7.08 (m, 1H), 6.85–7.00 (m, 1H), 6.60–6.78 (m, 2H), 3.59 (s, 8H, $OCH_2\underline{CH_2}O$), 3.49 (t, $^3J_{HH}$ = 5.4 Hz, $O\underline{CH_2}CH_2N$), 3.18 (t, $^3J_{HH}$ = 5.4 Hz, $OCH_2\underline{CH_2}N$).

2.5.3. Bis(diethyl-2,2′(phenylimino)diacetate)-diazacrown ether 3

To a solution of freshly prepared diamino derivative **2** (350 mg, 0.787 mmol) and proton sponge (843 mg, 5 eq) in 10 mL of acetonitrile was added diethyl iminodiacetate (510 µL, 5.5 eq). The resulting mixture was stirred at 80 °C overnight. The suspension was filtered on a Celite pad. The filtrate was evaporated to dryness. The residue dissolved in toluene was washed with HCl 0.1 M then water. The organic phase was decanted, dried on anhydrous Na_2SO_4 and evaporated to dryness. The desired compound **3** was isolated as a beige solid (355 mg, 57% yield) after purification of the crude by column chromatography on silica gel using dichloromethane/ethylacetate as eluent.

^{1}H NMR (250 MHz, $CDCl_3$): δ 7.16–7.25 (m, 2H), 6.89–7.02 (m, 6H), 4.27 (s, 8H, $N\underline{CH_2}COOEt$), 4.11 (q, $^3J_{HH}$ = 7.1 Hz, 8H, $\underline{CH_2}CH_3$), 3.45–3.67 (m, 16H, OCH_2CH_2N), 3.53 (s, 8H, OCH_2CH_2O), 1.21 (t, $^3J_{HH}$ = 7.1 Hz, 12H, $CH_2\underline{CH_3}$). ^{13}C NMR (62.5 MHz, $CDCl_3$): δ 171.1 (C = O), 142.8, 136.1, 123.7, 123.0, 120.5, 116.7, 70.4 and 69.6 (CH_2O crown ether), 60.4 ($N\underline{CH_2}CO_2Et$), 59.6 (NCH_2 crown ether), 55.1 ($\underline{CH_2}$–CH_3), 14.2 (CH_2–$\underline{CH_3}$). Elemental *Anal.*: Calc. for $C_{40}H_{60}N_4O_{12}\cdot 4\ CH_3CN$: C, 60.49; H, 7.61; N, 11.76. Found: C, 60.30; H, 7.80; N, 11.68%.

2.5.4. Bis(phenyliminodiacetate)-diazacrown ether 4

An aqueous solution of NaOH was added to a solution of **3** (120 mg, 0.152 mmol) in 5 mL of THF and the resulting mixture was stirred overnight at rt. The light-colored liquid phase above was decanted, and the oily residue was dried to give an off-white solid. **4** (rdt = 77%) ^{1}H NMR (250 MHz, D_2O): δ 7.37 (d, $^3J_{HH}$ = 7.8 - Hz, 2H), 7.03–7.09 (m, 2H), 6.95–7.01 (m, 2H), 6.91 (d, $^3J_{HH}$ = 7.3 - Hz, 2H), 4.05 (s, 8H, $\underline{CH_2}COO^-$), 3.54–3.69 (s, 24H, crown ether). ^{13}C NMR (62.5 MHz, $CDCl_3$): δ 179.9 (C carboxylate), 144.3, 139.3, 123.5, 123.1, 120.3, 118.6, 69.5 and 68.9 (CH_2O), 55.4 ($N\underline{CH_2}CO_2^-$), 50.8 ($N\underline{CH_2}CH_2O$). Elemental *Anal.* Calc. for $C_{32}H_{40}N_4Na_4O_{12}\cdot 4\ H_2O$: C, 45.94; H, 5.78; N, 6.70. Found: C, 46.01; H, 5.59; N, 7.06%.

2.6. X-ray structural determination

Slow diffusion of hexanes into a solution of **1** in dichloromethane gave yellow block crystals suitable for single-crystal X-ray diffraction. Suitable colorless prism-like crystals of **4-Ba** were grown by slow diffusion of acetone into an aqueous solution of $BaCl_2$:**4** (1:1) at room temperature. The data for **1** and **4-Ba** were collected on a Bruker APEX-II CCD X-ray diffractometer by using graphite-monochromated Mo Kα radiation (wavelength = 0.71073 Å). Unit-cell parameter determinations, data collection strategies, and integrations were carried out with the Bruker SAINT software [19]. The data were corrected from absorption by a multi-scan method [20]. The structures were solved by direct methods and refined by full-matrix least-squares on all F_0^2 data using SHELXS-97 [21] and SHELXL-97 [21,22]. All non-hydrogen atoms were refined anisotropically, and H atoms bonded to C atoms were placed at calculated positions. Crystallographic data and refinement details are presented in Table 3. Structural analyses and drawings were made using ORTEP-3 [23] and POV-ray 3.6 software.

3. Results and discussion

3.1. Synthesis

The synthesis of the novel macrocyclic derivative **4** was carried out in four steps from the commercially available diaza-18-crown-6. The synthetic route depicted in Scheme 1 starts with nucleophilic aromatic subsitution on o-fluoro-nitrobenzene which allowed the direct bis-arylation of the parent macrocycle in 90% yield. The nitro groups were reduced quantitatively to amino groups by catalytic hydrogenation with H_2 and Pd/C. Alkylation of the amino derivative **2** with ethyl-2-iodoacetate provided the desired proligand **3** in 57% yield. Subsequent alkaline hydrolysis of the tetrakis ester **3** yielded the corresponding tetrapotassium salt **4**.

All compounds except **2** were characterized by NMR spectroscopy and elemental analysis. In fact, the diamino derivative **2** which proved to be highly air-sensitive was characterized by ^{1}H NMR spectroscopy and then immediately subjected after workup to the following alkylation step.

The reduction of the nitro into amino group was clearly evidenced by ^{1}H NMR as significant highfield shiftings are measured for the methylene protons CH_2– ($\Delta\delta$ = −0.33 ppm) and the aromatic protons ($\Delta\delta$ = −0.65 ppm). The clean and complete conversion of the pro-ligand **3** into the corresponding tetraacetate ligand **4** was assessed by the disappearance of the triplet signal associated to ethyl ester group on the ^{1}H NMR spectrum and elemental analysis further confirmed the formation of **4**.

3.2. X-ray crystal structures

Single crystal X-ray structures were obtained for the pro-ligand **1** (see ESI) and a barium complex **4-Ba**. Representations of the molecular structures are shown in Figs. 1 and 2, and selected interatomic distances and angles for **4-Ba** are collected in Table 1.

Crystal structure of **4-Ba** shows an unusual complexation mode in such a way that the apparent stoichiometry in the solid state is $2L^{4-}$:$3Ba^{2+}$:$2Na^+$. Considering that there is a good match between Ba^{2+} ionic diameter and the size cavity of diaza-18-crown-6 ether, it was unexpected to localize all Ba^{2+} ions in the asymmetric unit out of the macrocylic cavity. The asymmetric unit (see Fig. 1) contains four distincts complexes involving Na^+ and Ba^{2+}.

Na^+ cation, located out of the macrocyclic cavity, is in a distorted octahedral environment where two acetate groups, two nitrogen atoms of o-phenylenediamine ring, one oxygen donor from the aza-crown ether are involved in the complexation (see Fig. 2). The coordination sphere for Na^+ is completed by one H_2O ligand that is further involved in hydrogen bonding to O8 in the crownether and O2 from acetate donor of the second phenylenediamine. The remaining three oxygen and nitrogen donors of the macrocycle are interacting neither with Na^+ nor with Ba^{2+}. The two nitrogen atoms N3 and N4 of the o-phenylenediamine interact nearly equally to Na^+ with bond lengths of 2.577(3) and 2.589(3) Å respectively. The average C–N–C bond angle for the macrocyclic amino group N3 (111°) and for the iminodiacetate group N4 (112°) points to a pyramidalization of both nitrogen atoms. This sp^3 hybridization originating from the perpendicular conformation adopted by the phenylenediamine with respect to the macrocycle, reinforces the basic character of the lone pairs allowing a stronger coordination of Na^+ cation. The average Na–O bond length is 2.355 Å with strong disparities between the various oxygen donors (ether, water and acetate) as shown in Table 1.

Three types of Ba^{2+} ions could be distinguished depending on their coordination environment. Ba1 is coordinated by nine donors arranged in a tricapped trigonal prism: four oxygen atoms

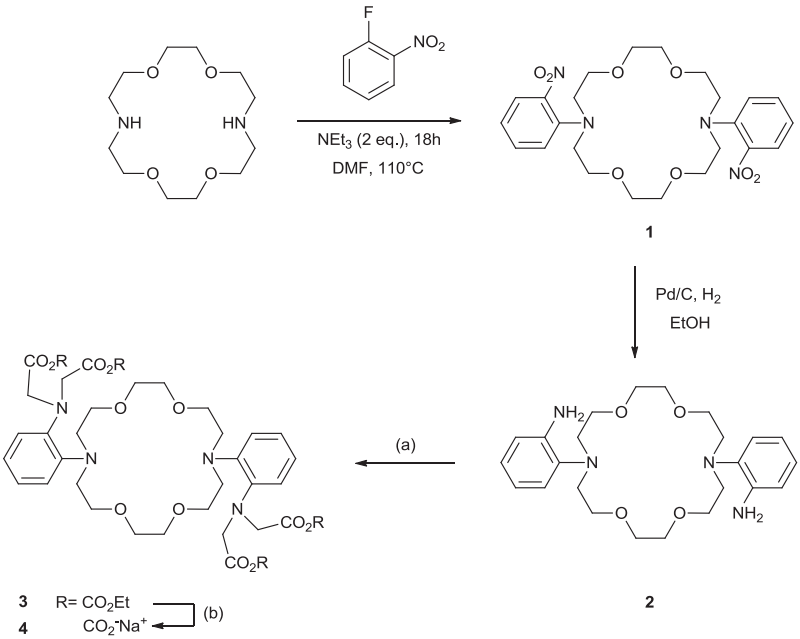

Scheme 1. Synthesis of Ligand **4**: (a) ethyl 2-iodoacetate, MeCN, reflux 24 h (57%); (b) NaOH, THF.

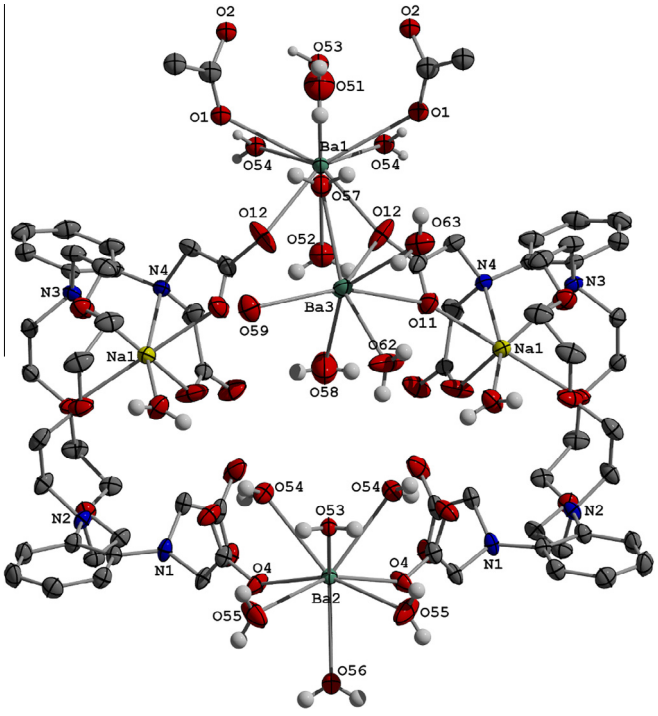

Fig. 1. Asymmetric unit in **4-Ba** showing the atom numbering scheme with the ellipsoids drawn at the 50% probability level. For the sake of clarity, hydrogen bonded to carbon atoms have been omitted.

(O1, O1_h, O12, O12_i) from four different acetate anions, five oxygen atoms (O51, O52, O53, O54, O54_h) from water molecules amongst which three are bridged with Ba2 (O53, O54, O54_h). Ba1-O bond distances range from 2.694 to 2.951 Å in accordance with reported barium complex structures [24–26]. Ba2 is octa-coordinated and located in bicapped trigonal prism. Two oxygen atoms (O4, O4_h) from acetate anions and four water molecules (O54, O54_e, O55, O55_h) occupy the corners of the trigonal prism. Two oxygen atoms (O53, O56) from water molecules cap two of the rectangular faces of the trigonal prism. The Ba3 cation is hepta-coordinated by two oxygen atoms (O11, O12) from one acetate in η^2 fashion and five oxygen atoms (O57, O58, O59, O62, O63) from water molecule. Although the bond distances Ba-O for **4-Ba** are consistent with those measured in previously reported azacrown ether crystal structures, it is worth mentionning that the stoichiometry 3:2 and the coordination environment for barium ions are unusual. [27–30] In fact, for crystals of diaza-18-crown-6-ether based complex grown in organic solvants, the most frequently encountered stoichiometry is 1:1 (Ba:L) where the barium cation is immersed within the macrocyclic cavity. In our case, **4-Ba** crystals were grown from an aqueous solution, and the peculiar solid state structure observed could originate from the strongly competing character of water ligand for hard metals like alkaline-earth.

3.3. UV–Vis spectrosopy

Affinity and selectivity of this new chelator were examined in aqueous solution by UV–Vis spectroscopy. In the absence of added cations, the ligand displays mainly three bands at 239, 263 and 300 nm. Spectral changes upon complexation provide the stoichiometry of complexation and its affinity constant. The titration of the tetra-anionic ligand with increasing amounts of Ba^{2+} ion is shown in Fig. 3. Ba^{2+} has been added until the absorbance intensity saturates. Similar trends are observed upon the addition of cations such as Ca^{2+}, Mg^{2+} or K^+ leading to the progressive decrease in intensity of the bands mentionned previously. Except for Ca^{2+}, all the studied cations follow the standard saturation behavior that would be expected for a simple 1:1 ligand: metal complexation (see Fig. S1–2 in the ESI). The stoichiometry of the barium complex was further confirmed by the Job's plot (see Fig. S3 in the ESI) whose apex point approximates 0.5. The absorbance values at two different wavelengths (263 and 239 nm) for various free cation concentrations were fitted with a 1:1 ligand: metal association model which allowed us to extract the affinity constants associated to these cations (Table 2).

The relative change in absorbance at 239 nm (Fig. 4) shows qualitatively that the affinity of the chelator for the studied cations decreases in the following order: $Ca^{2+} \gg Ba^{2+} > Mg^{2+} \gg K^+$. There is no clear correlation between the size of the cation and the affinity

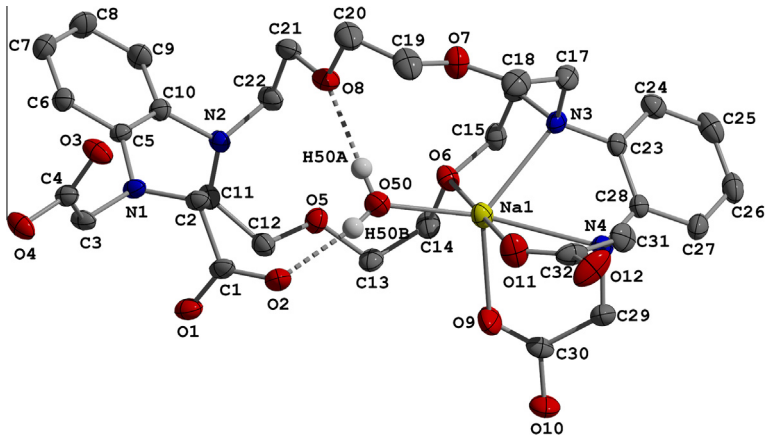

Fig. 2. Local coordination environment of Na^+ ion in **4-Ba** showing the atom numbering scheme with the ellipsoids drawn at the 50% probability level. For the sake of clarity, hydrogen atoms bonded to carbon atoms have been omitted.

Table 1
Selected bond lengths (Å) and angles (°) for **4-Ba**.

Na1–O6	2.485(2)	Na1–O50	2.286(3)
Na1–O9	2.315(3)	Na1–N3	2.577(3)
Na1–O11	2.333(3)	Na1–N4	2.589(3)
O50–O8	2.819(4)	O50–H50A–O8	178(5)
O50–O2	2.847(4)	O50–H50B–2	168(3)
O50–Na1–N4	162.34(10)	O6–Na1–O11	179.89(10)
O9–Na1–N3	126.85(10)		
Ba1–O1	2.951(2)	Ba1–O51	2.872(6)
Ba1–O52	2.860(5)	Ba1–O54	2.963(2)
Ba1–O53	2.907(4)	Ba1–O12_b	2.694(3)
Ba1–O1_h	2.951(2)	Ba1–O54_h	2.963(2)
Ba1–O12_i	2.694(3)		
Ba2–O4	2.751(2)	Ba2–O55	2.762(3)
Ba2–O56	2.852(4)	Ba2–O65	3.094(15)
Ba2–O53_c	2.775(3)	Ba2–O54_c	2.812(2)
Ba2–O54_e	2.812(2)	Ba2–O4–h	2.751(2)
Ba2–O55_h	2.762(3)		
Ba3–O62	2.815(7)	Ba3–O12	2.561(3)
Ba3–O63	2.807(7)	Ba3–O11	2.787(3)
Ba3–O58	2.728(7)	Ba3–O59	2.764(5)
Ba3–O57	2.782(4)		

Symmetry transformation codes: (b) $x, y, 1+z$; (c) $-1/2+x, 1/2-y, 5/2-z$; (e) $-1/2+x, y, 5/2-z$; (h) $x, 1/2-y, z$; (i) $x, 1/2-y, 1+z$.

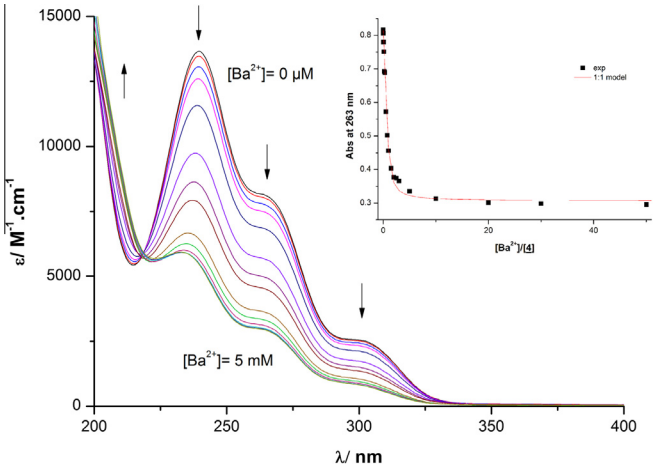

Fig. 3. UV–Vis spectra of compound **4** (100 µM) in water with increasing amount of barium (from 0 to 5 mM); (inset) Variation of the absorbance at 263 nm as a function of Ba^{2+} concentration. The solid line corresponds to the best fit of experimental data with the complexation model 1:1.

Table 2
Stability constants of Metal-ligand **4** complexes in water.

Cation	Ionic diameter* (Å)	Charge density* q ($Å^{-1}$)	Log*K*
Ba^{2+}	2.68	1.49	4.9
Ca^{2+}	1.98	2.02	N.D
K^+	2.66	0.75	3.9
Mg^{2+}	1.32	3.03	4.5

* See Ref. [31].

Table 3
Crystallographic data and refinement details for **1** and **4-Ba**.

	1	**4-Ba**
Formula	$C_{24}H_{32}N_4O_8$	$C_{64}H_{111}Ba_3N_8Na_2O_{42}$
Formula weight	504.54	2122.58
Crystal system	monoclinic	orthorhombic
Space group	*P* 21/*c*	*Pnma*
a (Å)	7.8791(6)	19.1396(6)
b (Å)	8.7413(7)	36.2618(12)
c (Å)	18.0281(14)	12.3022(4)
α (°)	90	90
β (°)	91.436(3)	90
γ (°)	90	90
V ($Å^3$)	1241.27(17)	8538.2(5)
Z	2	4
T (K)	200(2)	200(1)
λ (Å)	0.71073	0.71073
D_{calc} (g cm^{-3})	1.350	1.651
μ (mm^{-1})	0.102	1.476
Reflections collected	9619	50031
Independent reflections (R_{int})	3804 (0.0194)	13313 (0.0323)
Goodness-of-fit (GOF) on F^2	1.022	1.117
Final *R*, wR_2 [$I > 2\sigma(I)$]	0.0431, 0.1213	0.0463, 0.0969
All data	0.0623, 0.1330	0.0614, 0.1019

(see Table 2). In fact based on the ionic diameter, the size of potassium cation is almost the same as barium. Although being the smallest cation in the studied series, magnesium proved to be more strongly complexed by the ligand than potassium. The carboxylates when ionized provide a strong electrostatic field which greatly enhances the complex stability for alkali and alkaline earth metals. If we consider only the columbic forces, it becomes clear that a ligand with four anionic charges has a stronger interaction with divalent than with monovalent cations.

The titration curves for Ca^{2+} obtained by UV–Vis spectroscopy show clean isobestic points (at 202 and 215 nm) indicative of the co-existence of only two species in solution (the free ligand and the complex). However, the data points at a given wavelength

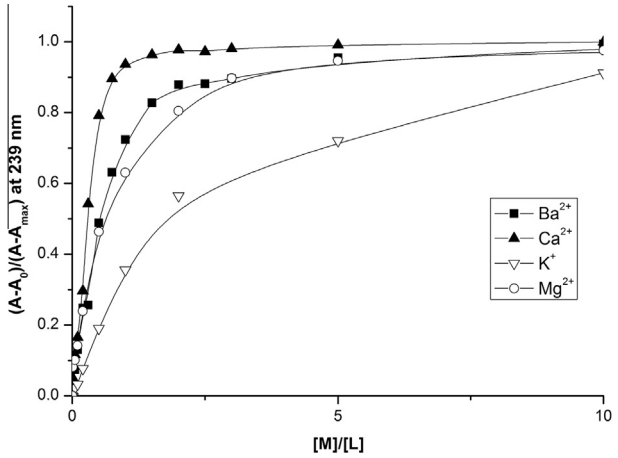

Fig. 4. Evolution of the normalized absorbance of ligand **4** in water with increasing amount of metal ion (Ba^{2+}, Ca^{2+}, K^+ or Mg^{2+}).

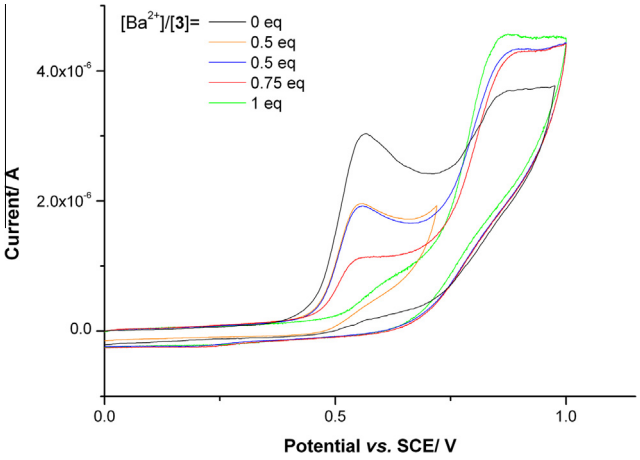

Fig. 6. Effect of Ba^{2+} concentration on the electrochemical response of **3** (1 mM) in acetonitrile solution (0.1 M nBu$_4$NBF$_4$). Scan rate: 100 mV s^{-1} on glassy carbon electrode (diameter = 1 mm).

follow a complex behavior (see inset Fig. 5) rather than the standard saturation curve that would be expected for a simple 1:1 stoichiometry. All attempts to fit the data points at a given wavelength with a 1:1 stoichiometry model (nonlinear least square analysis of the absorbance A versus the pre-equilibrium concentration c_M of Ca^{2+}) failed. The method of continuous variations applied for Ca^{2+} showed that the absorbance reaches a maximum at the mole fraction of 0.4 (see Job plot: Fig. S3 in the ESI). This value points to higher order association reaction such as $2L + 3M \leftrightarrow L_2M_3$. Despite being not very common, this stoichiometry is reasonable when considering the X-ray structure of the corresponding barium complex. From a quantitative point of view, calculation of the binding constant for stoichiometry other than 1:1 or 1:2, is more complicated because there is no explicit expression of the absorbance versus the total Ca^{2+} concentration c_M if the approximation $[Ca^{2+}] \approx c_M$ is not valid [31]. Therefore, we were not able to treat the data quantitatively to extract the affinity constant of **4** for Ca^{2+}.

3.4. Electrochemistry

The electrochemical properties of ligands **3** (see Fig. 6) and **4** (see Fig. S10 in ESI) were explored by cyclic voltammetry in acetonitrile and water respectively. The tetraester **3** has been successfully studied in the absence and in the presence of barium. Since the redox probe in **3** derives from an o-tetramethylphenylenediamine (o-TMPD), it is interesting to compare the electrochemical response of **3** to the parent o-TMPD whose redox behavior is well established in terms of reversibility and oxidation peak potentials (0.59 and 0.84 V versus SCE corresponding to the radical cation and dication formation respectively) [32].

The tetra-ester derivative **3** exhibits two irreversible oxidation peaks at 595 and 900 mV vs SCE at a scan rate of 100 mV/s. The first oxidation process assigned to the formation of the radical cation occurs at a comparable potential to o-TMPD but remains irreversible at all explored scan rates (0.1 to 5 V/s). Therefore, the replacement of two methyl groups of o-TMPD by a crown ether group has no effect on the oxidation potential but alters the stability of the o-phenylenediamine radical cation. This result differ from the electrochemical behavior of o-TMPD substituted azacrown ether reported by Sibert [33]. In that case, due to rapid conformational change the electron transfer is irreversible at low scan rate and reversible at faster scan rates ($v \geqslant 3$ V/s).

In the presence of increasing amounts of Ba^{2+}, a progressive decrease of the first redox peak of the free ligand is observed until a complete disparearence of this signal beyond one equivalent of Ba^{2+}. The electrochemical responses of chelators where complexation/decomplexation reactions are coupled to redox processes (square scheme mechanism) have been thoroughly studied by

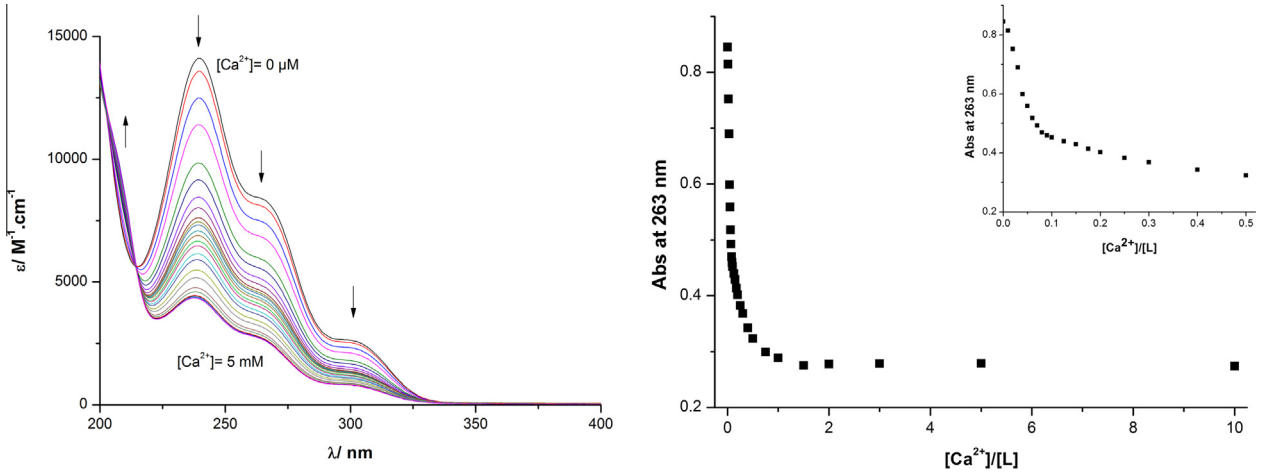

Fig. 5. (left). UV–Vis spectra of compound **4** (100 µM) in water with increasing amount of calcium (from 0 to 5 mM); (right) Variation of the absorbance at 263 nm as a function of Ca^{2+} concentration. Inset: Enlargement of the variation of the absorbance at low ratio $[Ca^{2+}]/[\mathbf{4}]$.

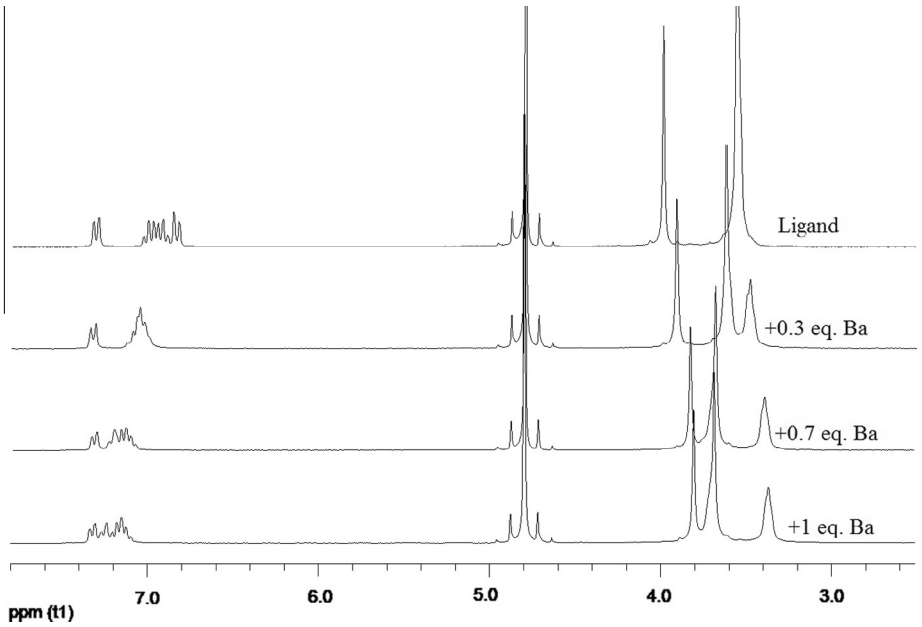

Fig. 7. ^{1}H NMR studies of barium complexation in D_2O.

means of theoretical and experimental tools. Two limiting electrochemical behaviors ("two-wave" versus "anodic shift") are described in the literature in the presence of sub-stoichiometric amounts of cations. The electrochemical response of **3** observed in the presence of sub-stoichiometric amount of Ba^{2+} differs widely from the reported electrochemical behavior of redox-active azacrown ether in the presence of substoichiometric amount of cation. For instance, ferrocenyl or o-TMPD substituted azacrown ether ligands exhibit an anodic-shift in the presence of increasing amount of cation. [33–36] The second oxidation wave of **3** in the presence of Ba^{2+} is barely affected suggesting a decomplexation of Ba^{2+} after the first redox process. Such barium decomplexation is the key step to release caged barium ions under electrochemical stimution as mentioned in the introduction of this paper.

3.5. NMR studies

To probe the effective participation of the potential donors in the cation coordination, ^{1}H NMR studies in deuterated water were conducted (see Fig. 7). The free ligand is characterized in the aliphatic region by overlapping multiplets at 3.55 ppm ($\underline{CH_2}$–N and $\underline{CH_2}$–O) and a singlet at 3.98 ppm ($N\underline{CH_2}$–CO_2^-). A gradual increase in Ba^{2+} concentration causes significant changes in the ^{1}H NMR spectrum with a progressive shifting of all resonance signals[1]. The magnitude of the shifting reaches a maximum at one equivalent of barium per ligand. Further increase in Ba^{2+} concentration has no significant effect on the chemical shifts, which is fully consistent with the 1:1 stoichiometry, as evidenced by UV–Vis. Upon addition of 0.1 equivalent of Ba^{2+} all the signals except one doublet in the aromatic region are shifted and the overlapping multiplets in the aliphatic region split into 2 signals. The resonance of the macrocyclic methylenes CH_2O protons are downfield shifted as a consequence of the chelation of barium ion. Such low field shift is due to the decrease of electron density on carbon adjacent to O-donor involved in Ba^{2+} complexation. Conversly, the macrocyclic methylenes CH_2N are highfield shifted in the presence of increasing amount of barium. This behavior which could seem unsual, is attributed to conformational changes in the crownether upon complex formation [26,29,37–39]. Depending on the relative conformation adopted by the diaminobenzene ring with respect to the diazacrown ether, the lone pair of N-donor will be more or less involved in the aromatic system thus modulating the Lewis basicity of the macrocyclic nitrogen lone pair. As a consequence, the nitrogen donor in perpendicular orientation with respect to the macrocycle, behaves more as a tertiary aliphatic amine than an aniline.

The methylenes $N\underline{CH_2}$–CO_2^- protons are significantly highfield shifted by 0.25 ppm suggesting that the second amino substituent (aminodiacetate) is also in a perpendicular orientation with respect to the phenyl ring. The substantial conformational rearrangement in the course of Ba^{2+} complexation due to the twisting of both nitrogen donors of the phenyl ring induces coherently the downfield shift of the aromatic protons.

The shifting of resonance peaks with increasing amount of Ba^{2+} in the medium was succesfully exploited to extract the affinity constant of ligand **4** towards Ba^{2+} in water ($\log K \approx 4.4$) and to confirm the expected 1:1 stoichiometry (see Fig. S9 in ESI). The affinity constants for Ba^{2+} determined by NMR and UV–Vis techniques are of the same order of magnitude and most importantly prove that the ligand **4** is well suited to operate in the millimolar concentration range required for the in vitro barium stimulation of cells.

4. Conclusions

In summary, a novel water soluble chelating agent intended to anther application than cation sensing has been designed and fully characterized. The affinity of this ligand towards commonly encountered metal ions in biological medium has been evaluated. Except for calcium, all other complexes have been characterized in solution as 1:1/M:L stoichiometry complexes. X-ray studies of the resulting crystalline barium complex showed that the apparent stoichiometry of the diazacrown ether in the solid state is not necessarly a reliable measure of the actual metal–ligand binding in solution. NMR and electrochemical studies revealed conformational rearrangement of the ligand upon complexation of barium ion and upon oxidation. The redox-induced barium release is currently investigated in our group.

[1] In the presence of, Ca^{2+}, the ^{1}H NMR spectrum proved to be hardly exploitable as all signals are broaden which points to a slow equilibrium compared to the time scale of, NMR experiment.

Acknowledgments

This work was supported by the CNRS (UMR 8640 and LIA XiamENS), ENS, the Université Pierre et Marie Curie. We thank Dr. Manon Guille Collignon and Dr. Frédéric Lemaître for the fruitful discussions about exocytosis cascade and cell stimulation.

Appendix A. Supplementary data

CCDC 940233–940234 contains the supplementary crystallographic data for **1** and **4-Ba**. These data can be obtained free of charge via http://www.ccdc.cam.ac.uk/conts/retrieving.html, or from the Cambridge Crystallographic Data Centre, 12 Union Road, Cambridge CB2 1EZ, UK; fax: (+44) 1223-336-033; or e-mail: deposit@ccdc.cam.ac.uk. Supplementary data associated with this article can be found, in the online version, at http://dx.doi.org/10.1016/j.poly.2013.10.024.

References

[1] G.C.R. Ellis-Davies, Chem. Rev. 108 (2008) 1603.
[2] K.L. Haas, K.J. Franz, Chem. Rev. 109 (2009) 4921.
[3] C. Amatore, S. Arbault, M. Guille, F. Lemaitre, Chem. Rev. 108 (2008) 2585.
[4] C. Amatore, S. Arbault, I. Bonifas, M. Guille, Biophys. Chem. 143 (2009) 124.
[5] D.A. Przywara, P.S. Chowdhury, S.V. Bhave, T.D. Wakade, A.R. Wakade, Proc. Natl. Acad. Sci. USA 90 (1993) 557.
[6] T.S. Sihra, D. Piomelli, R.A. Nichols, J. Neurochem. 61 (1993) 1220.
[7] M. Verhage, J.J.H. Hens, P.N.E. DeGraan, F. Boomsma, V.M. Wiegant, F.H.L. daSilva, W.H. Gispen, W. Ghijsen, Eur. J. Pharmacol. Mol. Pharmacol. Sect. 291 (1995) 387.
[8] S.R. Adams, J.P.Y. Kao, G. Grynkiewicz, A. Minta, R.Y. Tsien, J. Am. Chem. Soc. 110 (1988) 3212.
[9] J.P.Y. Kao, R.Y. Tsien, Biophys. J. 53 (1988) 635.
[10] S.R. Adams, J.P.Y. Kao, R.Y. Tsien, J. Am. Chem. Soc. 111 (1989) 7957.
[11] K.X. Bhattacharyya, L. Boubekeur-Lecaque, I. Tapsoba, E. Maisonhaute, B. Schollhorn, C. Amatore, Chem. Commun. 47 (2011) 5199.
[12] K.X. Bhattacharyya, L. Boubekeur-Lecaque, I. Tapsoba, E. Maisonhaute, B. Schöllhorn, C. Amatore, Dalton Trans. 41 (2012) 14257.
[13] P.N. Basa, A. Bhowmick, M.M. Schulz, A.G. Sykes, J. Org. Chem. 76 (2011) 7866.
[14] P.D. Beer, P.A. Gale, G.Z. Chen, Coord. Chem. Rev. 186 (1999) 3.
[15] S.R. Miller, D.A. Gustowski, Z.H. Chen, G.W. Gokel, L. Echegoyen, A.E. Kaifer, Anal. Chem. 60 (1988) 2021.
[16] A.E. kaifer, S. Mendoza, Redox Switchable Receptors, in: G.W. Gokel (Ed.), Comprehensive Supramolecular Chemistry, Elsevier, New York, 1996, p. 701.
[17] A. Anantanarayan, T.M. Fyles, Can. J. Chem. 68 (1990) 1338.
[18] M. Tazaki, K. Nita, M. Takagi, K. Ueno, Chem. Lett. (1982) 571.
[19] Bruker APEX2 and SAINT, in, Bruker AXS, Madison, Wisconsin, USA, 2009.
[20] R.H. Blessing, Acta Crystallogr., Sect. A 51 (1995) 33.
[21] G.M. Sheldrick, SHELXS-97, Program for Crystal Structure Resolution, in, Univ. of Göttingen: Göttingen, Germany, 1997.
[22] G.M. Sheldrick, SHELXL-97, Program for Crystal Structure Analysis, in, Univ. of Göttingen: Göttingen, Germany, 1997.
[23] L.J. Farrugia, J. Appl. Crystallogr. 30 (1997) 565.
[24] N.K. Dalley, G.P. Xue, J.S. Bradshaw, X.X. Zhang, R.G. Harrison, P.B. Savage, K.E. Krakowiak, R.M. Izatt, J. Heterocycl. Chem. 38 (2001) 1.
[25] T. Maity, D. Saha, S. Das, S. Koner, Eur. J. Inorg. Chem. (2012) 4914.
[26] L.K. Minacheva, P.K. Sazonov, V.S. Sergienko, G.A. Artamkina, I.P. Beletskaya, A.Y. Tsivadze, Russ. J. Inorg. Chem. 51 (2006) 1071.
[27] M.V. Alfimov, A.V. Churakov, Y.V. Fedorov, O.A. Fedorova, S.P. Gromov, R.E. Hester, J.A.K. Howard, L.G. Kuzmina, I.K. Lednev, J.N. Moore, J. Chem. Soc., Perkin Trans. 2 (1997) 2249.
[28] P.K. Sazonov, G.A. Artamkina, I.P. Beletskaya, Russ. J. Org. Chem. 42 (2006) 438.
[29] P.K. Sazonov, L.K. Minacheva, A.V. Churakov, V.S. Sergienko, G.A. Artamkina, Y.F. Oprunenko, I.P. Beletskaya, Dalton Trans. (2009) 843.
[30] A. Rodriguez-Rodriguez, I. Carreira-Barral, M. Regueiro-Figueroa, D. Esteban-Gomez, C. Platas-Iglesias, A. de Blas, T. Rodriguez-Blas, Polyhedron 31 (2012) 402.
[31] B. Valeur, In: Molecular Fluorescence. Principles and Applications, Wiley–VCH, Weinheim, 2002. p. 337.
[32] S.F. Nelsen, E.L. Clennan, L. Echegoyan, L.A. Grezzo, J. Org. Chem. 43 (1978) 2621.
[33] J.W. Sibert, P.B. Forshee, Inorg. Chem. 41 (2002) 5928.
[34] P.D. Beer, C. Blackburn, J.F. Mcaleer, H. Sikanyika, Inorg. Chem. 29 (1990) 378.
[35] P.D. Beer, Z. Chen, M.I. Ogden, J. Chem. Soc., Faraday Trans. 91 (1995) 295.
[36] Z. Chen, A.J. Pilgrim, P.D. Beer, J. Chem. Soc., Faraday Trans. 91 (1995) 4331.
[37] J.W. Sibert, D.J. Seyer, G.R. Hundt, J. Supramol. Chem. 2 (2002) 335.
[38] J.W. Sibert, P.B. Forshee, G.R. Hundt, A.L. Sargent, S.G. Bott, V. Lynch, Inorg. Chem. 46 (2007) 10913.
[39] A.L. Sargent, B.J. Mosley, J.W. Sibert, J. Phys. Chem. A 110 (2006) 3826.